

# Lateral Dye-Sensitized Microscale Solar Cells via Femtosecond Laser Patterning

Xi Zhang, Yinggang Huang, Hao Bian, Hwei Liu, Xuezheng Huang, and Hongrui Jiang\*

Low cost, high efficiency, long-term stability, and excellent scalability are features that researchers always pursue for solar cells. Dye-sensitized solar cells (DSSCs) are considered to have a great potential to achieve all these goals.<sup>[1,2]</sup> Conventional DSSCs have a sandwiched structure in which charge transport occurs perpendicular to the device surface, as shown in **Figure 1a**. Recently, solar cells with lateral structures<sup>[3–8]</sup> have caught much attention owing to the following advantages in comparison with the conventional vertical structure: (a) The necessity of the transparency of the electrode can be eliminated; both electrodes can be placed at the back side and use high-conductivity materials, while the light can be incident from the front. As a result, transmission loss can be reduced and the charge collection increased simultaneously. (b) Compact device structure can be realized that is more conducive to scaling up, integration, and functionalization. (c) Flexible devices are feasible. Lateral DSSC is, therefore, a concept of advanced structure of DSSCs with lateral transport of charges, as shown in **Figure 1b**. A few structures have been proposed in this direction. Back-contact structure, which leads both photoelectrode (PE) and counter electrode (CE) to the back side of the device, was developed from monolithic structure<sup>[9]</sup> to interdigital structure<sup>[10,11]</sup> in recent years, as shown in **Figure 1c,d**, respectively. In a back-contact DSSC in **Figure 1d**, CE of Pt/fluorine-doped tin oxide (FTO) was interdigitally patterned and separated from PE made of TiO<sub>2</sub>, which was about 10 μm thick and not patterned.<sup>[10]</sup> Therefore, most of the photoinduced charges still transport vertically in such back-contact structure, while a small number of carriers transport laterally in a limited region near PE, which has a nanoscale thickness. Li et al. reported a DSSC structure that realized lateral PE-CE separation (**Figure 1e**), which is so far the closest structure to the lateral DSSCs.<sup>[3]</sup> However, in their structure, the Pt layer has intrinsically nanoscale thickness, which is much less than the thickness of the neighboring PE. Such structure along with the limited PE material of ZnO nanowire resulted in a low performance of the solar cell. In this study, we accomplished lateral DSSCs with patterned PE and CE as shown in **Figure 1b**.

Currently, the research on lateral structures for the emerging new-generation solar cells other than DSSCs, including organic photovoltaics (OPVs) and perovskite solar cells (PSCs), is also being conducted. Nevertheless, the best photon-to-electron conversion efficiency ( $\eta$ ) of these lateral solar cells is still very low: 0.5% for OPVs<sup>[5]</sup> and 1.88% for PSCs.<sup>[7]</sup> Lateral DSSC is not an exception, with  $\eta$  less than 1%.<sup>[3]</sup> One of the common issues of these low-efficiency lateral solar cells is their low fill factor (FF) of less than 0.3.<sup>[3–8]</sup> It indicates that the fundamental problem of great internal loss in these lateral structures is still hard to overcome. In this work, we utilized the powerful femtosecond (fs) laser to directly pattern nano-TiO<sub>2</sub>/FTO photoelectrode into microscale units and successfully obtained lateral DSSCs with the best  $\eta$  of 5.18%, much better than the previously reported lateral solar cells. FF achieved of this lateral DSSC was nearly 0.6.

Fs laser ablation has proven to be a convenient and effective method to create micro- or nano-structures in bulk materials<sup>[12–15]</sup> and nano materials,<sup>[16–18]</sup> and is especially advantageous to create high aspect ratio structure.<sup>[15]</sup> In this study, we utilized fs laser to cut through the nanoporous TiO<sub>2</sub> film on the FTO glass substrate and scan within the TiO<sub>2</sub> region to construct an interdigital pattern, where the used-to-be PE was divided into two electrodes, both consisting of microscale fingers. One of the separated electrodes was deposited with Pt by electrodeposition to form the CE of the lateral DSSC, while the other electrode was loaded with dye molecules as the PE. The ion transport between neighboring PE and CE fingers is thus in a completely lateral mode, as shown in **Figure 1b**. One such solar cell is formed by a number of sub-cells with microscale fingers, the merit of which lies in that the subcells could be rearranged and connected for functionalization as individual microscale modules.<sup>[19,20]</sup> The spacer-free structure could avoid possible contact in practice between the electrodes. The lateral PE-CE structure of nanostructured TiO<sub>2</sub> could also be directly implemented in quantum dot-sensitized solar cells (QDSSCs)<sup>[21]</sup> that possess a very similar device structure to that of DSSCs. This compact lateral design could substantially reduce the structural complication of devices such as tandem solar cells<sup>[22,23]</sup> and hybrid solar energy harvesting/storage devices.<sup>[24,25]</sup>

In order to demonstrate the ultra-compactness of this lateral microstructure, we also applied this lateral micro-design to fabricate a tandem DSSC with an unprecedented electrolyte-interconnected structure in which a lateral top cell and a lateral bottom cell were vertically combined. As a result, we obtained a type of tandem DSSC with a structure as compact as a single DSSC, owing to the ultra-compactness of the lateral DSSC. In comparison with traditional tandem DSSCs,<sup>[23]</sup> such lateral tandem DSSC has the simplest structure and realizes considerable performance with a  $\eta$  of 6.21%.

Dr. X. Zhang, Y. Huang, Dr. H. Bian, Dr. H. Liu,  
Dr. X. Huang, Prof. H. Jiang  
Materials Science and Engineering  
Department of Electrical and Computer Engineering  
University of Wisconsin-Madison  
Madison, WI 53706, USA  
E-mail: hongrui@engr.wisc.edu



DOI: 10.1002/admt.201600121

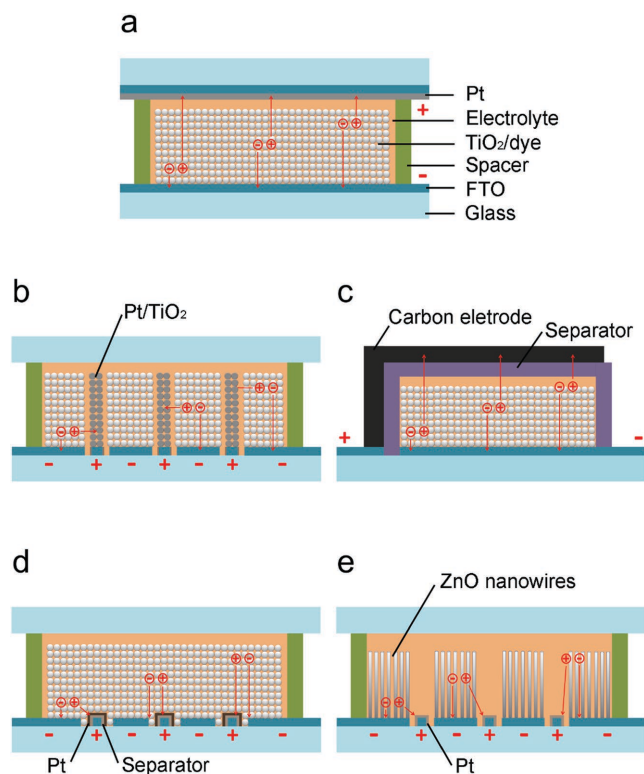


**Figure 1.** a) Conventional sandwich-structured DSSC, b) lateral DSSC with patterned PE (-) and CE (+), c) monolithic back-contact DSSC, d) back-contact DSSC with patterned CE, e) lateral DSSC with hierarchical PE and CE. Photogenerated positive and negative charges are shown in each structure.

The fabrication process of the lateral DSSCs is shown in Figure 2a–e. The 10  $\mu\text{m}$  thick nanostructured  $\text{TiO}_2$  film was deposited onto an FTO glass substrate first, followed by sintering at 500  $^\circ\text{C}$ , as shown in Figure 2a. Using a laser ablation system, linearly polarized 700 fs laser pulses were sent to an objective lens and subsequently focused onto the sample surface with a fixed spot size of 1.5  $\mu\text{m}$  diameter. The optimized pulse energy is 4.2  $\mu\text{J}$ , which could adequately cut through the  $\text{TiO}_2/\text{FTO}$  layer all the way to the glass substrate. An interdigital pattern was defined with the width of a PE finger (100  $\mu\text{m}$ ) larger than that of a CE finger (35  $\mu\text{m}$ ). By scanning the laser beam along the programmed paths (Figure 2b), PE and CE were separated and isolated. The scanning electron microscopy (SEM) image of the patterned  $\text{TiO}_2/\text{FTO}$  glass is shown in Figure 2f, while the microscopic image of the whole film is shown in Figure S1a (Supporting Information). The cross-sectional SEM images in Figure 3a,b show that the fs laser formed a V-shaped profile all through the  $\text{TiO}_2$  layer. The width at the top of the  $\text{TiO}_2$  film was 8.3  $\mu\text{m}$ , while the width at the bottom was 2.9  $\mu\text{m}$ . The average spacing between neighboring PE and CE fingers was about 5.6  $\mu\text{m}$ , lower than the spacing (typically  $\approx 15 \mu\text{m}$ ) between the vertical PE and CE in conventional DSSCs. This smaller spacing could improve the ion transport in the electrolyte of DSSCs, and contribute to the improvement of the overall performance.<sup>[26]</sup> The morphology detail near the ablated region in Figure 3b,c shows that most of the ablated  $\text{TiO}_2$  particles with a laser energy

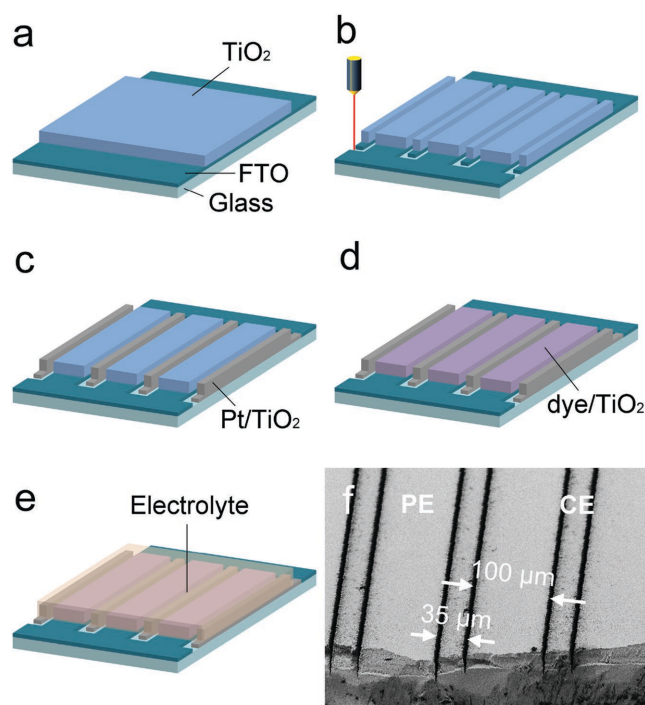


**Figure 2.** Schematics of the fabrication process of the lateral DSSC: a) nanostructured  $\text{TiO}_2$  film deposited on FTO glass, b)  $\text{TiO}_2/\text{FTO}$  patterned by femtosecond laser ablation, c) electrodeposition of Pt on CE fingers, d) dye-loading on PE fingers, e) electrolyte filling and device sealing. f) SEM image of the tilted top view of the laser-patterned  $\text{TiO}_2$  film, where the widths of patterned fingers are labeled.

of 4.2  $\mu\text{J pulse}^{-1}$  were removed, and no distinct damage or alteration to the nanoporous  $\text{TiO}_2$  could be observed. An X-ray diffraction (XRD) characterization of the  $\text{TiO}_2$  nanoparticles before and after the ablation at 4.2  $\mu\text{J pulse}^{-1}$  shows that ablation under such level of pulse energy did not

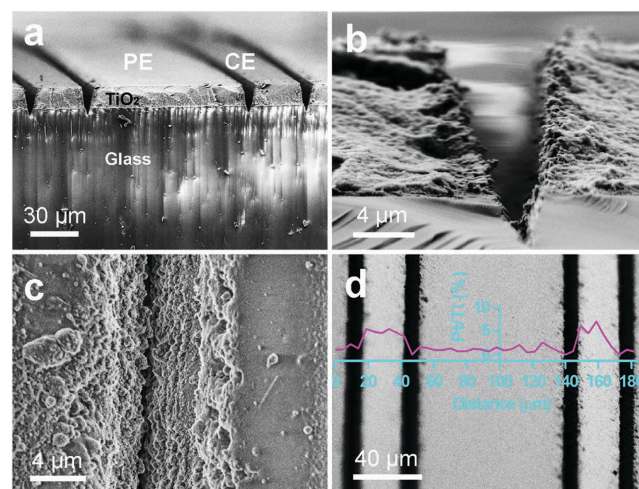


**Figure 3.** a) Cross-sectional SEM image of laser-patterned  $\text{TiO}_2$  film, where CE fingers are deposited with Pt. Cross-sectional and top view images of one ablation channel are shown in b,c), respectively. d) Top view SEM image of patterned  $\text{TiO}_2$  film with Pt, where the line-scanning curve of EDS is shown, with the atomic ratio of Pt/Ti as the y-axis.

change the anatase lattice, as shown in Figure S2 (Supporting Information).

Next, the patterned region of the sample was dipped into a  $\text{PtClO}_4$  aqueous solution to deposit Pt onto the narrow CE fingers, as shown in Figure 2c. In order to characterize the deposited Pt on CE fingers, energy dispersive x-ray spectrometry (EDS) analysis was performed. The line-scanning on the top surface of the  $\text{TiO}_2$  film was conducted and the results are shown in Figure 3d. Most of the Pt was distributed on the CE area between the two ablated channels, with a portion of about 6% in comparison with Ti. Pt also appeared at the edge of the PE, but with limited width of about  $3\ \mu\text{m}$ . Hence Pt could be well controlled to be loaded only onto the narrow  $\text{TiO}_2$  fingers as CE of the lateral DSSC. This Pt deposition process is sensitive to the laser-patterning with microscale spacing between neighboring PE and CE fingers. When the laser energy is lower, this spacing is reduced. However, too small a spacing could result in short-circuit by the  $\text{PtClO}_4$  solution during the electrodeposition and some of the Pt could be deposited onto the PE fingers, which would have a negative impact on the device performance, as shown in Figure S3 (Supporting Information). On the other hand, higher laser energy, for example  $4.6\ \mu\text{J pulse}^{-1}$  under the same conditions, was inferior too: it was found that the  $\text{TiO}_2$  film could crack.

After Pt deposition, the PE was loaded with dye and the film was filled with electrolyte and sealed, as shown in Figure 2d,e. An organic dye of RK1,<sup>[27]</sup> which has a superior performance for wavelengths below 600 nm, was utilized. The current density–voltage ( $J$ – $V$ ) results of a lateral DSSC and a reference DSSC with a traditional structure under AM 1.5G illumination are shown in Figure 4a, while all the corresponding parameters were listed in Table 1. For the tests of the lateral DSSC, the incident light was from the back side of the device. The photocurrent density, short-circuit photocurrent density ( $J_{\text{sc}}$ ), and  $\eta$  of each lateral cell in this work were calculated based on the area of the PE region, where the incident light is harvested and converted to carriers. Hence the defined internal  $J_{\text{sc}}$  and  $\eta$  for lateral DSSCs reflect the real photon-to-electron conversion performance of the PE material. If considering the CE part that is exposed to the incident light yet does not generate current, external  $J_{\text{sc}}$  and  $\eta$  of the overall device should be reduced by 26% (from the area ratio of 35:100 between PE and CE) and the corresponding results are shown in Table S1 (Supporting Information). Therefore, the area portion of CE in the design should be as low as possible while maintaining its function. Such lateral structure is especially suitable for the photovoltaic (PV) system with concentrators,<sup>[19,28]</sup> where the CE-induced light harvesting loss could be completely avoided.

From Figure 4a,  $J_{\text{sc}}$  of the lateral DSSC is close to that of the reference DSSC with the same dye and PE material/thickness, indicating that the photo harvesting and conversion performance of PE were well preserved during the laser patterning. FF, which reflects the internal loss of photovoltaic devices,<sup>[29–31]</sup> was reduced from 0.687 to 0.569, indicating that the charge recombination and internal loss in the cell are close to but moderately higher than those in the conventional DSSCs. These losses might stem from the edges of the CE fingers, where the laser process was experienced and some Pt was deposited

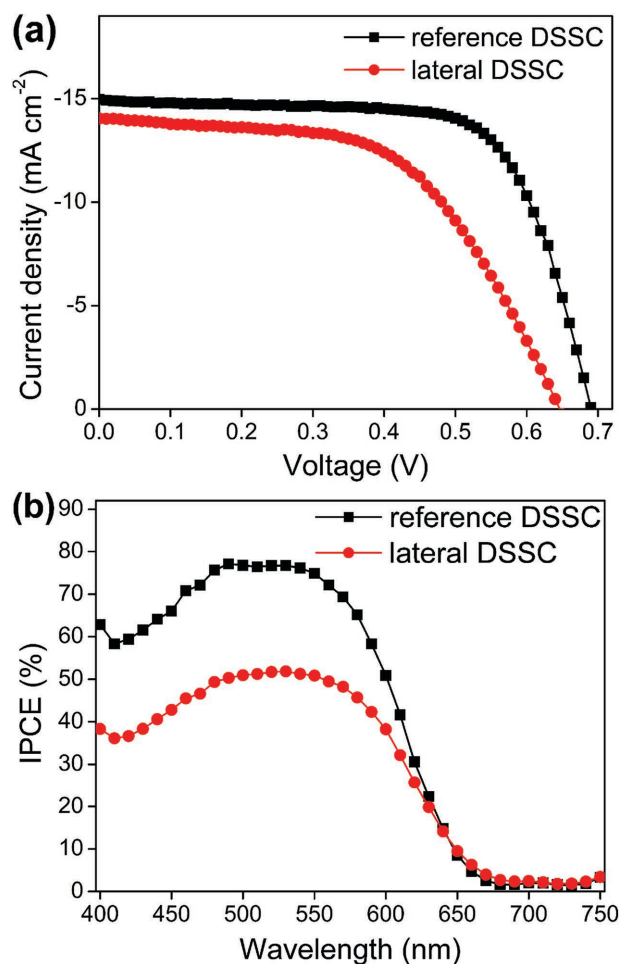


**Figure 4.** a)  $J$ – $V$  curves and b) IPCE spectra of a conventional DSSC and a lateral DSSC with back incident light.

as shown in Figure 3d. In comparison with previous work on lateral DSSC in Reference [3], the performance of this lateral DSSC is significantly improved. Its performance is also much greater than that of other types of lateral solar cells,<sup>[4–8]</sup> where low levels of FF limited the overall performance of the devices. The much improved FF in this lateral DSSC overcame most internal loss of the photovoltaic process and accounted for the great improvement in  $\eta$ . The open-circuit voltage ( $V_{\text{oc}}$ ) of the

**Table 1.**  $J$ – $V$  parameters of all the DSSCs in this work.

Cell (dye)	$V_{\text{oc}}$ [V]	$J_{\text{sc}}$ [ $\text{mA cm}^{-2}$ ]*	FF [%]	$\eta$ [%]*
Reference (RK1)	0.70	15.0	68.7	7.20
Lateral (RK1)	0.65	14.0	56.9	5.18
Tandem	0.63	17.0	58.1	6.21
Top (RK1)	0.65	14.1	56.4	5.17
Bottom (N719)	0.57	3.48	55.0	1.09

\* $J_{\text{sc}}$  and  $\eta$  of lateral cells were calculated based on the area of PE, which is 74% of the device area exposed to the AM 1.5G illumination.

lateral DSSC was measured to be 0.65 V, slightly lower than 0.70 V of the reference DSSC. The most probable origin of this lowering is also the imperfect fringe area of the PE fingers. The results of the incident photon-to-current efficiency (IPCE) measurements from the 400 to 750 nm wavelength range are shown in Figure 4b. IPCE of the lateral DSSC is lower than that of the reference DSSC, while the shape of the spectrum remained the same after laser patterning. The IPCE decay of the lateral DSSC seems larger than the  $J_{sc}$  reduction in Figure 4a. This is because the IPCE spectrum of the lateral DSSC was obtained based on the whole area of the incident light spot, which contains the areas of both PE and CE. Therefore, the real IPCE values afforded by the PE of the lateral DSSC should be 1.35 times of the result in Figure 4b, and should be much closer to the IPCE of the reference DSSC.

A promising application of the lateral PE-CE structure is the fabrication of tandem solar cells. Applying the novel lateral PE-CE structure in tandem DSSCs could eliminate this interlayer in conventional tandem DSSCs,<sup>[23]</sup> as shown in Figure 5a. Such tremendous simplification of the tandem DSSC structure could increase the incident light reaching the bottom cell and facilitate the device fabrication. The two subcells in one such tandem DSSC share the same electrolyte; thus the two subcells need to be connected in parallel when this tandem cell is running. RK1 dye was used in the top cell, while N719 dye was used in the bottom cell to supplement the long wavelength absorption of the device. The TiO<sub>2</sub> film and patterning parameters of the two subcells are the same. The incident light through the tandem cell is from the back to the front side of the top cell, while from the front to the back side for the bottom cell. The measured  $J$ - $V$  curves of the top cell, the bottom cell, and the tandem cell under AM 1.5G are shown in Figure 5b and the parameters are listed in Table 1.  $\eta$  of this tandem lateral DSSC reached 6.21%, 19.9% greater than that of the single lateral DSSC. The performance of the top cell is the same as a single lateral DSSC with light incident from the bottom side. The  $V_{oc}$  value of the tandem DSSC is between that of the top cell and that of the bottom cell, due to the parallel connection of the two subcells.  $J_{sc}$  of the tandem cell agrees well with the summation of those of the top and bottom cells. The corresponding normalized IPCE spectra of the tandem cell and subcells are shown in Figure 5c. The IPCE spectrum of the tandem DSSC is in agreement with the combination of those of the two subcells, resulting in its summed  $J_{sc}$  from the two subcells. The photo-harvesting supplement at wavelengths longer than 600 nm by the dye N719 from the bottom cell effectively extends the spectral range of the light converted for this tandem DSSC. These results show that the tandem DSSC based on lateral PE-CE structure could well expand the spectrum of harvested light with an ultracompact device architecture. Better spectrum matching and device optimization will further boost the overall performance of such tandem solar cells.

In conclusion, we created a lateral PE-CE structure of nanostructured TiO<sub>2</sub>/FTO films with microscale interdigital fingers for DSSCs through a facile process of a one-step femtosecond laser patterning. The performance of this lateral DSSC, especially FF, was significantly improved in comparison with other types of laterally structured third-generation solar cells. The compact lateral DSSCs greatly

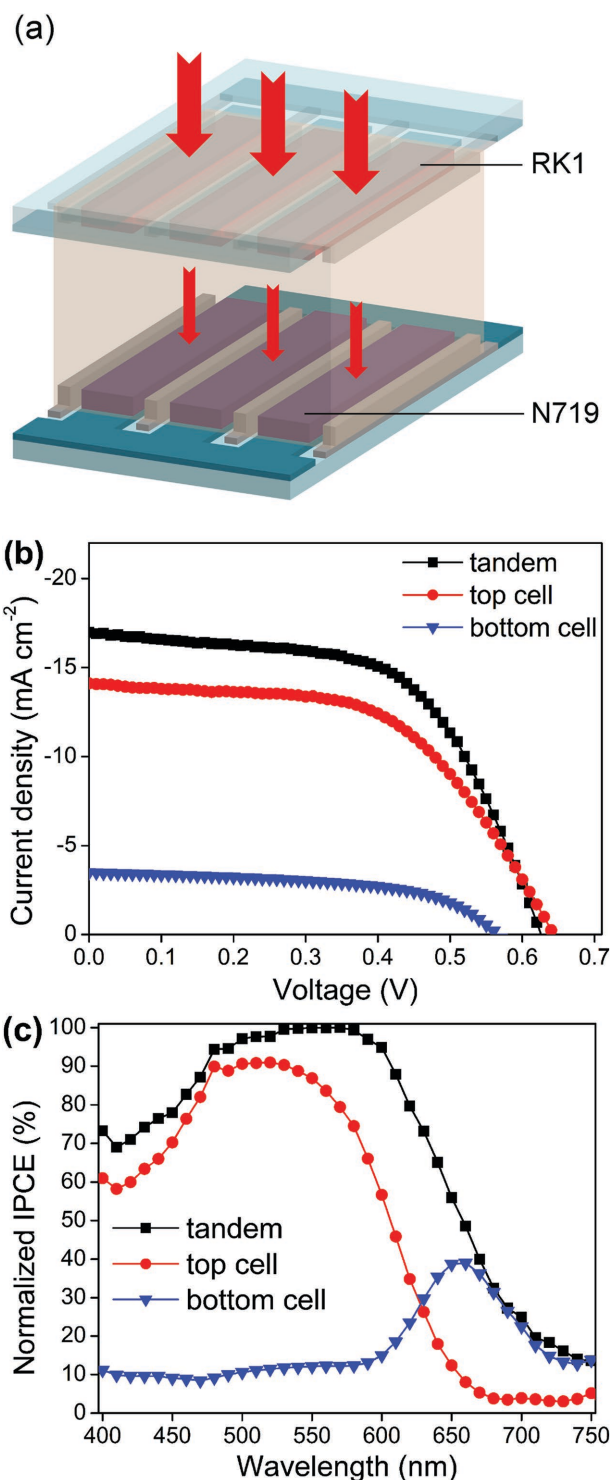


**Figure 5.** a) Schematic of the tandem lateral DSSC with patterned TiO<sub>2</sub> photoelectrode by laser ablation. b)  $J$ - $V$  curves of a lateral tandem DSSC and its subcells. c) Normalized IPCE spectral comparison of a lateral tandem DSSC and its subcells.

simplified the structure of tandem DSSCs. The design of this lateral structure with microscale interdigital fingers could be directly implemented in QDSSCs, and the laser patterning

of microscale-thickness films could be applied to other types of solar cells, such as interdigital PEs for OPVs and PSCs. Furthermore, by applying this lateral TiO<sub>2</sub> PE-CE structure, we obtained the most compact tandem structure in comparison with the state-of-the-art tandem DSSCs. Such lateral-structure-based tandem DSSCs with top and bottom cells in parallel showed impressive spectrum widening and improvement in  $J_{sc}$  and  $\eta$ . The design of such lateral DSSCs also has great potential in flexible solar cells, concentrator-PV system, mini PV modules, and integrated/hybrid micro electronics. The successful application of this lateral PE-CE structure in tandem DSSCs paves a promising path to multifunctions and high performance of solar cells. In our future work, we will focus on the individual electrode finger and study its surface variation by laser processing to further improve the performance of such lateral DSSCs.

## Experimental Section

10  $\mu\text{m}$  thick transparent TiO<sub>2</sub> film consisting of 20 nm TiO<sub>2</sub> nanoparticles (Solaronix, Switzerland) was deposited onto FTO glass (1.5 cm  $\times$  1.5 cm, TEC-15, MTI Co.) using a doctor-blade method before being sintered at 500 °C. The area of the circular TiO<sub>2</sub> active region on the FTO glass was 0.15 cm<sup>2</sup>. For the bottom cell of the tandem DSSC, the TiO<sub>2</sub> film was deposited on FTO glass with two holes drilled for electrolyte filling.

A vertically polarized laser (Uranus2000-1030-1000, PolarOnyx) at the wavelength of 1030 nm, with a pulse duration of 700 fs and a repetition rate of 120 kHz, was delivered into an objective lens (N.A. = 0.8, Nikon) and focused on the sample surface. The diameter of the focal spot was 1.5  $\mu\text{m}$ . A mechanical shutter was used to turn the laser on and off. A neutral density attenuator and a polarizer were used to control the power and polarization of the laser beam. The sample was mounted on a computer-controlled xyz stage (Newport XMS-160, XMS-100 and GTS-30V for the x-axis, y-axis and z-axis, respectively). By translating the sample, the microstructure was ablated by the focused laser pulses, and a CCD camera and a relay lens were used for real-time monitoring of the ablation process. The scanning speed was 1 mm s<sup>-1</sup>.

The ablated TiO<sub>2</sub> film was then cleaned with deionized water and dried before being immersed into a 0.5 M H<sub>2</sub>PtCl<sub>6</sub> aqueous solution. Pt was deposited onto the CE of the film under three 2V-constant-bias pulses (pulse width: 10 s, rest time: 30 s) via an electrodeposition process. The films were subsequently sintered at 500 °C for 1 h. After being cooled down to 120 °C, it was soaked into the dye solutions (0.3  $\times$  10<sup>-3</sup> M RK1 (Solaronix, Switzerland) in acetonitrile-tert-butanol, v/v = 1:1, or 0.3  $\times$  10<sup>-3</sup> M N719 (Solaronix, Switzerland) in acetonitrile-tert-butanol, v/v = 1:1 for the bottom cell of the tandem DSSC) and kept at room temperature for 24 h. The CE was Pt-coated FTO glass with two drilled holes for filling the electrolyte. A 25  $\mu\text{m}$  thick Surlyn (Solaronix, Switzerland) film was used as a spacer between the PE and the CE for each DSSC. The redox electrolyte contained 0.1 M LiI, 0.05 M I<sub>2</sub>, and 0.6 M 1,2-dimethyl-3-propylimidazolium iodide, using acetonitrile as solvent.

The morphology of the patterned TiO<sub>2</sub> films and deposited Pt in the interdigital CE were characterized by SEM with EDS (Zeiss LEO 1530). XRD spectra of TiO<sub>2</sub> films were measured by a Bruker/Siemens Hi-Star 2d X-ray diffractometer with a monochromatic Cu K-alpha point source (0.8 mm). The  $J$ - $V$  measurements of the DSSCs were performed using a Keithley 2400 source meter under the illumination of simulated AM 1.5G solar light (Oriel 94022A equipped with a 150W Xe lamp and an AM 1.5G filter). A 0.12 cm<sup>2</sup> circular mask was used for all the  $J$ - $V$  tests. For the IPCE measurement,  $J_{sc}$  of DSSCs at each wavelength in the range of 400–750 nm was recorded by the Keithley 2400 source meter before the IPCE values were calculated. The light from the Oriel 94022A light source was delivered

through a monochromator (Mini-Chrom 300–800 nm, Edmund Optics) and illuminated the DSSCs. The wavelength step was set at 10 nm.

## Supporting Information

Supporting Information is available from the Wiley Online Library or from the author.

## Acknowledgements

This work was supported by the US National Institute of Health (Grant No. 1DP2OD008678-01). H.B. thanks the support from the State Scholarship Fund of the China Scholarship Council (CSC; Grant No. 201406285050). This research utilized the US National Science Foundation supported shared facilities at the University of Wisconsin.

Received: June 14, 2016

Revised: July 6, 2016

Published online:

- [1] M. Grätzel, R. A. J. Janssen, D. B. Mitzi, E. H. Sargent, *Nature* **2012**, 488, 304.
- [2] S. Mathew, A. Yella, P. Gao, R. Humphry-Baker, B. F. Curchod, N. Ashari-Astani, I. Tavernelli, U. Rothlisberger, M. K. Nazeeruddin, M. Grätzel, *Nat. Chem.* **2014**, 6, 242.
- [3] H. Li, Q. Zhao, W. Wang, H. Dong, D. S. Xu, G. J. Zou, H. L. Duan, D. P. Yu, *Nano Lett.* **2013**, 13, 1271.
- [4] M. Kim, S. B. Jo, J. H. Park, K. Cho, *Nano Energy* **2015**, 18, 97.
- [5] M. Kim, J. H. Park, J. H. Kim, J. H. Sung, S. B. Jo, M.-H. Jo, K. Cho, *Adv. Energy Mater.* **2015**, 5, 1401317.
- [6] Z. Xiao, Y. Yuan, Y. Shao, Q. Wang, Q. Dong, C. Bi, P. Sharma, A. Gruverman, J. Huang, *Nat. Mater.* **2015**, 14, 193.
- [7] Q. Dong, J. Song, Y. Fang, Y. Shao, S. Ducharme, J. Huang, *Adv. Mater.* **2016**, 28, 2816.
- [8] A. Ahnood, H. Zhou, Y. Suzuki, R. Sliz, T. Fabritius, A. Nathan, G. A. J. Amaratunga, *Nanoscale Res. Lett.* **2015**, 10, 486.
- [9] H. Han, U. Bach, Y. Cheng, R. A. Caruso, C. MacRae, *Appl. Phys. Lett.* **2009**, 94, 103102.
- [10] D. Fu, X. L. Zhang, R. L. Barber, U. Bach, *Adv. Mater.* **2010**, 22, 4270.
- [11] H. Yang, D. Fu, M. Jiang, J. Duan, F. Zhang, X. Zeng, U. Bach, *Thin Solid Films* **2013**, 531, 519.
- [12] M. Shen, J. E. Carey, C. H. Crouch, M. Kandyla, H. A. Stone, E. Mazur, *Nano Lett.* **2008**, 8, 2087.
- [13] M. Farsari, B. N. Chichkov, *Nat. Photonics* **2009**, 3, 450.
- [14] U. Zywietz, A. B. Evlyukhin, C. Reinhardt, B. N. Chichkov, *Nat. Commun.* **2014**, 5, 3402.
- [15] H. Liu, Y. Huang, H. Jiang, *PNAS* **2016**, 113, 3982.
- [16] X. Zhang, H. Liu, X. Huang, H. Jiang, *J. Mater. Chem. C* **2015**, 3, 3336.
- [17] X. Huang, H. Liu, X. Zhang, H. Jiang, *ACS Appl. Mater. Interfaces* **2015**, 7, 27845.
- [18] G. Mincuzzi, A. L. Palma, A. Di Carlo, T. M. Brown, *ChemElectroChem* **2016**, 3, 9.
- [19] X. Sheng, C. A. Bower, S. Bonafede, J. W. Wilson, B. Fisher, M. Meitl, H. Yuen, S. Wang, L. Shen, A. R. Banks, C. J. Corcoran, R. G. Nuzzo, S. Burroughs, J. A. Rogers, *Nat. Mater.* **2014**, 13, 593.
- [20] P. Kubis, N. Li, T. Stubhan, F. Machui, G. J. Matt, M. M. Voigt, C. J. Brabec, *Prog. Photovolt: Res. Appl.* **2015**, 23, 238.
- [21] I. J. Kramer, E. H. Sargent, *Chem. Rev.* **2014**, 114, 863.

- [22] W.-S. Jeong, J.-W. Lee, S. Jung, J. H. Yun, N.-G. Park, *Sol. Energy Mater. Sol. Cells* **2011**, 95, 3419.
- [23] S. K. Balasingam, M. Lee, M. G. Kang, Y. Jun, *Chem. Commun.* **2013**, 49, 1471.
- [24] X. Zhang, X. Huang, C. Li, H. Jiang, *Adv. Mater.* **2013**, 25, 4093.
- [25] D. Schmidt, M. Hager, U. Schubert, *Adv. Energy Mater.* **2016**, 6, 1500369.
- [26] S. Ito, S. M. Zakeeruddin, P. Comte, P. Liska, D. Kuang, M. Grätzel, *Nat. Photonics* **2008**, 2, 693.
- [27] D. Joly, L. Pellejà, S. Narbey, F. Oswald, J. Chiron, J. N. Clifford, E. Palomares, R. Demadrille, *Sci. Rep.* **2014**, 4, 4033.
- [28] M. Peng, S. Hou, H. Wu, Q. Yang, X. Cai, X. Yu, K. Yan, H. Hu, F. Zhu, D. Zou, *J. Mater. Chem. A* **2014**, 2, 926.
- [29] X. Zhang, S.-T. Wang, Z.-S. Wang, *Appl. Phys. Lett.* **2011**, 99, 113503.
- [30] L. Y. Han, A. Fukui, Y. Chiba, A. Islam, R. Komiya, N. Fuke, N. Koide, R. Yamanaka, M. Shimizu, *Appl. Phys. Lett.* **2004**, 84, 2433.
- [31] F. Fabregat-Santiago, J. Bisquert, E. Palomares, L. Otero, D. Kuang, S. M. Zakeeruddin, M. Grätzel, *J. Phys. Chem. C* **2007**, 111, 6550.
-